

## Article

# Hydrodynamic Study of a Hybrid Electro-Flotation Column

Polyxeni K. Tsavé, Margaritis Kostoglou \*, Nikolaos K. Lazaridis and Thodoris D. Karapantsios \*

Laboratory of Chemical and Environmental Technology, School of Chemistry, Aristotle University of Thessaloniki, GR-541 24 Thessaloniki, Greece; tsavpoly@chem.auth.gr (P.K.T.); nlazarid@chem.auth.gr (N.K.L.)

\* Correspondence: kostoglou@chem.auth.gr (M.K.); karapant@chem.auth.gr (T.D.K.)

**Abstract:** Bubble columns are used in the mining industry for mineral recovery but are also widely utilized in the chemical and petrochemical industry. The hydrodynamic characteristics of their performance is a field of interest with a number of points, which are nonetheless poorly understood, and a considerable amount of methods have aimed to shed light on the flow regimes that prevail in the columns. The study of the hydrodynamic part of a flotation process should consider characteristics such as air flow, volumetric gas fraction, flow field, and bubble size, along with the mechanical and design factors and pulp properties. The present work aims to elucidate the characteristics of the gas phase of a hybrid flotation system. For this purpose, a hybrid flotation column was designed and constructed and the bubbles size distributions at different radial positions in the flotation column were computed by analyzing high resolution digital images. A patented electrical impedance technique was employed to instantaneously measure the local volumetric gas fraction. Flow dispersion in the column was studied by residence time distributions using conductivity tracers. The experimental results are discussed to comprehend the variation in the gas fraction in the column. In particular, the study showed that the size of the bubbles changed from the center to the walls of the column, and this was observed both radically and vertically. Moreover, the size of the bubbles affected the volume fractions, and no coalescence of the bubbles was observed. Finally, the dispersion of the tracer in the working solution was distributed uniformly in the volume of the column, with a time difference for the four positions of the column.



**Citation:** Tsavé, P.K.; Kostoglou, M.; Lazaridis, N.K.; Karapantsios, T.D. Hydrodynamic Study of a Hybrid Electro-Flotation Column. *Minerals* **2024**, *14*, 344. <https://doi.org/10.3390/min14040344>

Academic Editors: Bingqiao Yang, Weijun Peng and Shulei Li

Received: 18 February 2024

Revised: 19 March 2024

Accepted: 22 March 2024

Published: 26 March 2024



**Copyright:** © 2024 by the authors. Licensee MDPI, Basel, Switzerland. This article is an open access article distributed under the terms and conditions of the Creative Commons Attribution (CC BY) license (<https://creativecommons.org/licenses/by/4.0/>).

**Keywords:** froth flotation; hydrodynamics; column; combined flotation; electrolysis; fine particles

## 1. Introduction

The most important parameters that affect a flotation process are the slurry chemistry and the hydrodynamics of the phenomenon [1]. The performance of a flotation column is affected by the characteristics of the flow field [2] and, moreover, importance is also paid to the “micro-hydrodynamics” observed due to the lack of homogeneity with the appearance of the local turbulent flow, which is responsible for the bubble–particle interactions and flotation kinetics [3].

Studies have shown that the presence of the gas phase changes the local characteristics of the flow [4–6], while suspended fine solid particles can prevent the generation of turbulent flow [5,7]. Therefore, the study of the hydrodynamic part of a flotation process should consider characteristics such as air flow, volumetric gas fraction, and bubble size, along with the mechanical and design factors and pulp properties.

Air flow (or superficial gas velocity) is an extremely important parameter in the flotation process [8]. In mechanical flotation devices, the apparent velocity is recommended to not exceed 3 cm/s, because at higher values, the efficiency of the process decreases and entrainment is observed [9]; meanwhile, values smaller than 1 cm/s reduce the kinetics of flotation. In general, air flow affects the air dispersion, bubble size, and volumetric gas fraction [10]. Higher air flow rate values result in a lower particle residence time in the froth zone, preventing bubble coalescence [11]. This leads to an increase in yield, as the coalescence of bubbles is one of the reasons for the detachment of the particles from the

bubbles. In addition, increasing the air flow also increases the surface area of the bubbles, enhancing the probability of particle to bubble collision [12]. At large values, a reduction in the efficiency of flotation is caused, provoking entrainment. Finally, on the other hand, low air flow leads to the opposite results and, more specifically, to the rupture of the bubbles in the foam phase and thus to a reduction in recovery [12]. Values of 0.01–0.03 m/s are considered optimal gas velocity values for industrial scale columns. Increasing the air volume fraction up to a point can improve the flotation kinetics; however, at high values (>30%) it leads to a decrease in efficiency [13]. Furthermore, increasing the apparent velocity leads to entrainment of the solid particles, reducing the selectivity of the process [14].

Most early studies of the flow in the flotation columns assumed that laminar flow dominated. A significant amount of older research stated that the flow velocity in the center of a column was upward, whereas near the walls it faced downward [15]. Furthermore, Xia et al. established that the gas–liquid flow in the column could cause turbulent pulsation [16]. Recently, the prediction and evaluation of these parameters have been managed utilizing CFD simulations. This approach allows for the simulation of various experimental conditions in different flotation devices, such as the Denver [17], Jameson cell [18], or flotation column [19]. Flow fields have been studied throughout the years and developments in experimental fluid dynamics (EFDs) and computational fluid dynamics (CFDs) have been managed. Particle image velocimetry (PIV) is an advanced EFD-based velocity measurement method that was developed in the late 1970s. In general, the flotation process is accompanied by turbulent flow, independent of the flotation devices. In a turbulent flow field, mineral particles interrelate with the bubbles instantly after the injection of the gas phase in the system. Several models have been reported that describe the turbulence in a flotation system, such as  $k-\varepsilon$ ,  $k-\omega$ , Reynolds stress model, and large eddies simulations. Additionally, the simulation of the multiphase flow can be modeled with either the Eulerian–Langrangian or the Eulerian–Eulerian approach. The former considers that the fluid is a continuous medium and the bubbles and particles are discrete phases, whereas the latter considers continuous and dispersed phases as continuous media that can penetrate each other. It is important to consider that precise liquid–phase hydrodynamic properties can be achieved from the numerical simulation of the single-phase flow. Yet, the requirements for the prediction of the flotation efficiency cannot be assembled by the single-phase flow simulation.

The size of the bubbles is crucial for the successful recovery of mineral particles with regards to the technique of flotation. For instance, microbubbles have a lower relative velocity, which offers a number of advantages for the flotation of fine particles. For a constant volume of air in the cell, as the bubble size decreases, the number of bubbles increases noticeably and leads to an increase in collision probability. Furthermore, decreasing the bubble size increases the gas hold-up and increases the bubble concentration, which leads to an increase in the probability of bubble–particle collision. To that end, the bubble size and shape has been studied extensively over the past years and frameworks for a number of techniques have been developed. The most common methods to measure conventional-sized bubbles are optical and photographic techniques [20], image analysis [21,22], and electrical impedance [23,24]. There are a large body of experimental data that confirm that the use micro or nano bubbles enhance the recovery of fine mineral particles. To that end, recently, a number of techniques have been developed that can be utilized for measuring micro and nano bubble size distributions. Among these methods are laser pulse methods [25], nanoparticle tracking analysis [26,27], laser-diffraction-based technologies and dynamic light scattering (DLS) [28] X-ray techniques [29], and indirect measurements through dissolved oxygen reverse estimation [30].

Several techniques have been developed that aim to measure the volumetric gas fraction in a two-phase flow. Among them are capacitance sensors [31], magnetic resonance [32,33], ultrasonic methods [34,35], radiation attenuation techniques [36,37], and wire mesh sensors [38,39]. The void fraction in a two-phase flow can also be measured by applying acoustic emission technology for measuring acoustic emission signals. The

most widely used method is the optical method, as it is non-intrusive and accurate. The measurements are made using high-speed cameras and tomography algorithms. In previous studies [40,41], it was found that the laser transmittance varies with the area of the gas–liquid surface when an infrared laser beam passes through the gas–liquid two-phase flow. Information about the gas void fraction of the two-phase flow can be derived from the laser transmittance. Another method is the electrical capacitance tomography technique, which images the two-phase flow in a pressurized pipeline and is used for industrial applications [42]. In addition, electrical impedance tomography is a method that was introduced in past decades it results in accurate estimations of the local gas phase dispersed in a liquid medium, taking into account the local axial, radial, and angular components of the dispersed phase [43].

Bubble columns are widely used in the chemical, mining, and petrochemical industry and the hydrodynamic characteristics of their performance is a field of interest with a number of aspects that are still poorly understood. Recently, a considerable amount of work has been devoted to developing methods that aim to understand the flow regimes that prevail in columns. Among these methods is the radioactive particle technique (RPT), which is used to obtain flow measurements [44]. Two non-intrusive methods for two-phase flow study are the laser doppler velocimetry (LDV) [37,38] and the particle image velocimetry (PIV) [45–48]. Experimental data derived from these methods show that the flow field in a system with bubble evolution could be transformed from laminar to turbulent.

The scope of the work is the construction of a hybrid flotation column that generates *in situ* microbubbles, by employing electrolysis of water in order to study and characterize the hydrodynamics of the combined microflotation. To this end, the structure of this work is as follows: first, the bubble size distributions are determined by capturing photos of both conventional and electrolytic bubbles, and their size is calculated using custom-made image analysis software. Then, the turbidity of the flotation medium is estimated by employing a scattered light method. The gas holdup is determined by utilizing an electrical technique that estimates the volumetric gas fraction in the current flotation system. Finally, an NaCl solution serves as a conductivity tracer for the estimation of the residence time distributions in an effort to study the mixing conditions inside the flotation column.

## 2. Materials and Methods

### 2.1. Experimental Set Up—The Hybrid Flotation Column

The laboratory device used for mineral flotation in the present study was a laboratory scale custom constructed column (Figure 1). The flotation column consisted of three plexiglas cylindrical sections, connected with two flanges, and it was completely sealed. Plexiglas is a preferential material used for laboratory-scale flotation columns mainly due to its stability and, moreover, it can also be used for three-phase flow observation.

The column's height was 60 cm, its diameter was 7 cm, and the width of the walls was 3 mm. At the top of the flotation column, around the outer surface, a concentric cylindrical overflow weir was mounted where the recovered particles were collected. The column could be divided into two zones (Figure 1b): the collection zone, where particles collided with the air bubbles and the froth zone, where the recovered particles were collected.

Two boron-doped diamond (BDD) electrodes served as an electrolysis unit, as described in a previous study [49]. The unit was supported on the inner wall of the flotation column, 6 cm above the column's bottom (Figure 2), so that the produced microbubbles could be dispersed homogeneously in the column's volume. The electrodes were placed horizontally and parallel and connected to an external power supply. There are many studies indicating that combining conventional-sized bubbles with microbubbles leads to enhancing the fine particle recovery [50–52]. The hybrid column was capable of producing bubbles with an average bubble diameter less than 40 and over 400  $\mu\text{m}$ , enhancing the flotation of fine mineral particles.

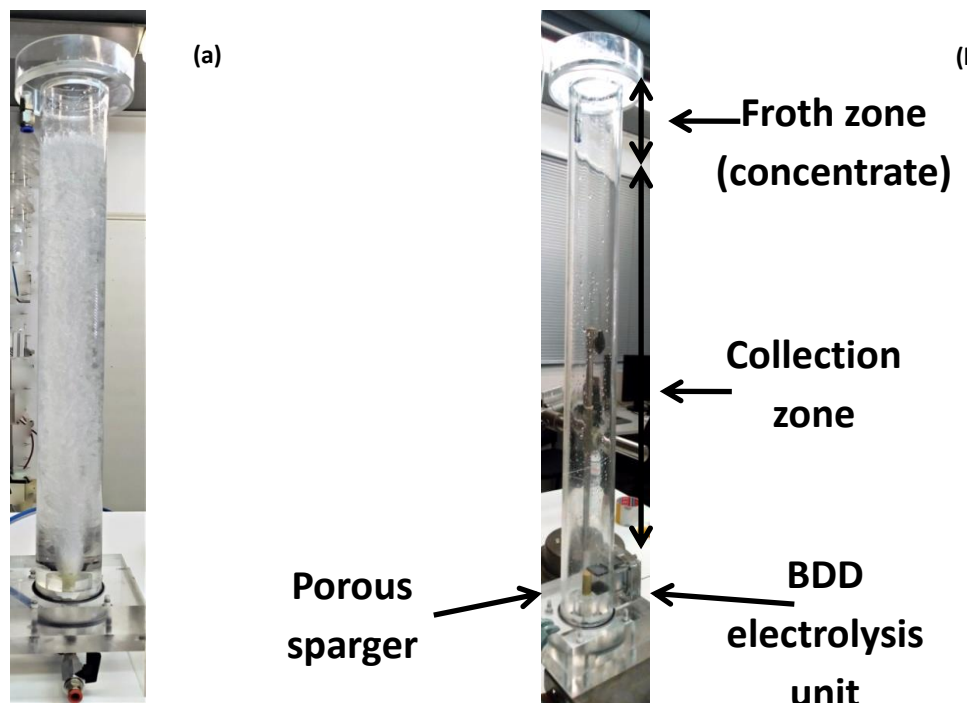


**Figure 1.** (a) The flotation column and (b) the hybrid electroflotation column.

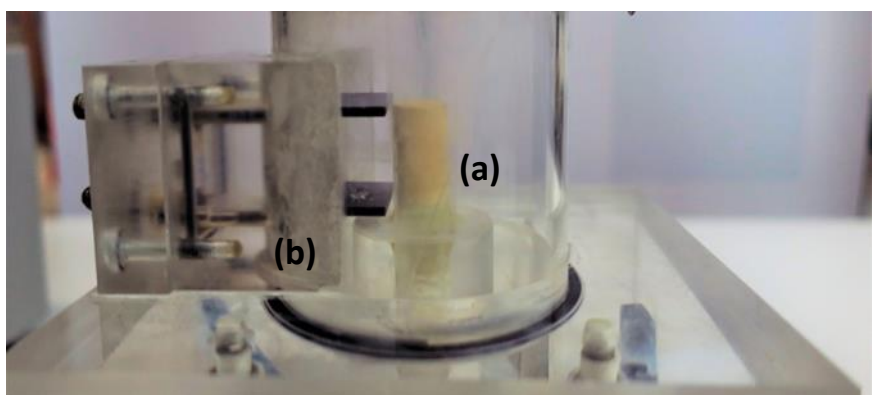


**Figure 2.** (a) Ceramic porous sparger and (b) BDD electrolysis unit.

Given the fact that the gas phase of a flotation system is crucial for the successful attachment of mineral particles onto bubbles, experiments for measuring the size and number of the bubbles involved in the flotation slurry were conducted. The gas fraction involved in the flotation process was characterized using both optical and electrical methods. The optical methods were employed to determine the bubble size distributions and turbidity of the flotation medium (correlation of bubbles size and number), whereas the electrical diagnostic techniques were involved in the determination of the volumetric fraction of the gas bubbles.

#### Materials and Reagents

The frother used in this research was the anionic surfactant sodium oleate ( $\text{NaOl}$ ,  $\geq 82\%$  fatty acids, Riedel-de Haen, Seelze, Germany). The pH was adjusted using 0.1 M  $\text{NaOH}/\text{HCl}$  (Pancreac); moreover, pine oil was employed as the frother to improve the stability of the froth [53]. Sodium chloride ( $\text{NaCl}$ ; VWR Chemicals, Radnor, PA, USA) was utilized as a background electrolyte, and throughout the flotation experiments dionized

water ( $\sim 10 \mu\text{S}/\text{cm}$ ) was used. The experiments were conducted on the aforementioned hybrid electroflotation column.

## 2.2. Diagnostic Techniques

### 2.2.1. Optical Measurements—Bubble Size Distributions

The size of the bubbles was determined by capturing the bubble images using a high resolution digital camera (a 20 MP Canon EOS 70, Tokyo, Japan) equipped with macro lenses and extension tubes for efficient image magnification (Figure 3). A custom-made image analysis software (BubbleSEdit software) was used to automatically detect the contour of the bubbles and to measure their size and consequently obtain the corresponding bubble size distributions [54].



**Figure 3.** Camera for the optical measurements.

It is worth mentioning that in order to calculate the size of the bubbles from the photos taken, it is necessary to convert the pixels to  $\mu\text{m}$ . The calibration of the optical measurements was achieved by capturing a standard  $56 \mu\text{m}$  thick wire with the camera settings used per the experimental conditions. Moreover, the possible alteration of the dimensions of  $x,y$  inside the flotation column in the presence of water was taken into consideration.

### 2.2.2. Intensity of Bubbles-Induced Scattered Light Method

An optical system (Intensity of bubbles-Induced Scattered Light method) was able to estimate the turbidity of the flotation medium by measuring the intensity of the light that passed from one side to the opposite side of the flotation cell (non-intrusive measurements) [55]. The change in light intensity due to scattering was related to the formation of bubbles in the two-phase system. The factors determining this change were the number and size of the dispersed air bubbles. The optical measurement system consisted of a cold light source placed on one side of the flotation device, while a photodetector was placed on the other side of the device (S121C, Thorlabs Inc., Newton, NJ, USA), which was connected to a computer via USB and power meter software (PM101 Photodiode and Thermal Power Sensor Interface with USB, RS232 (Thorlabs GmbH (Lübeck), Lübeck, Germany)) (Figure 4). For the measurement, a frequency generator was used and the current was adjusted and remained constant, so that any change in the intensity of the light recorded by the sensor was only due to its diffusion.

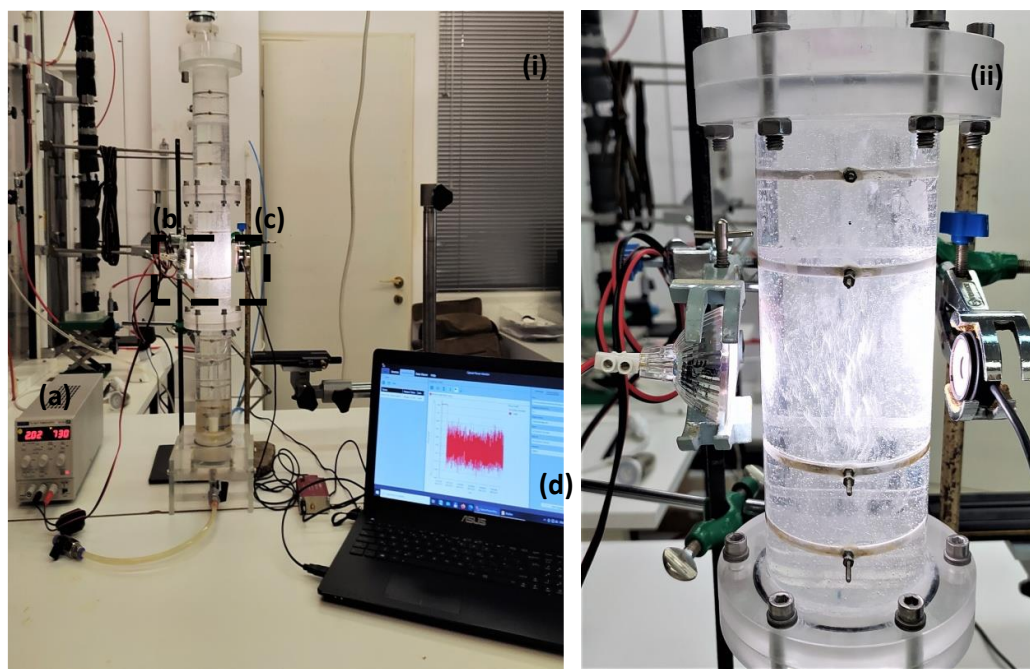


**Figure 4.** (i) Experimental set up for the optical intensity of bubbles-induced scattered light method: (a) generator, (b) light source, (c) light detector, and (d) laptop for the data acquisition and processing. (ii) Close up photo of the light source (b) and detector (c).

### 2.2.3. Electrical Technique—Gas Fraction Measurements

The electrical technique was employed to determine the volumetric gas fraction in the current flotation system. The gas holdup parameter affected the flotation performance and defined the bubble-flow density, which was mostly related to the flotation kinetics [56]. The estimation of the gas holdup at different locations on the flotation column could be established with a unique patented method called I-VED, which is an electrical spectroscopy impedance technique with multiplexer technology (Figure 5) [57].

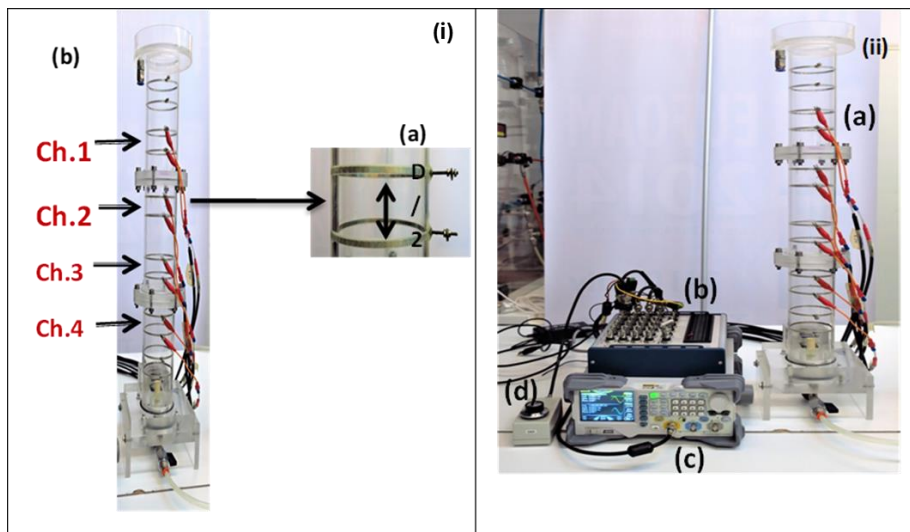


**Figure 5.** (i) (a) The annular electrodes in the channel for measuring the electrical impedance of the passing medium and (b) the four different channels along columns height for measuring the volumetric gas fraction with multiplex technology. (ii) Experimental set up for the electrical measurements: (a) electrical impedance technique I-VED with multiplexer technology, (b) data acquisition card, (c) digital multimeter, and (d) terminal resistance.

The technique measured the ohmic component of electrical impedance, which is equivalent to the electrical resistance or vice versa of the electrical conductivity of the medium. The principle of the present technique is based on the fact that the formation of a gas phase (non-conductive) in a liquid volume (conductive phase), increases the electrical resistance (or equivalently reduces the electrical impedance) of the medium. The change in electrical resistance was affected by the quality characteristics of the bubbles, such as their size and number. The current technique permitted the evolution of local volumetric gas fraction during the flotation process. This expanded the single-point information by showing, in real time, the dispersion of the gas phase along the column height. Electrical impedance of the studied flotation medium occurred by employing metallic electrodes that were placed in pairs along the column's height (Ch1–4, Figure 5i(a)). The distance between the electrodes of each pair was 32 mm (Figure 5i(a)) and corresponded to  $D/2$  of the column (where  $D$  is the inner diameter of the column). According to previous experimental data [58,59], an electrode distance equal to  $D/2$  ensured the radial homogeneity of the impedance measurements, while maintaining the local behavior of the measurement for the corresponding column height. The impedance measured was the equivalent intervening between the opposed electrodes. The electrical impedance data obtained during measurement were transformed into gas fraction time series using Maxwell's model. Measurements were conducted at a frequency of 25 kHz in order to electrically excite the flow inside the column, generating an input current passing through the medium. Experimental data indicated that an excitation frequency of 25 kHz provided almost pure resistive behavior.

The present diagnostic technique took advantage of the fact that the electrical impedance of the medium used in the flotation runs decreased in the presence of air (gas phase). Therefore, the difference in the measured impedance of the flotation medium, before and after the introduction of air, could be transformed to the gas phase evolution in time and height.

The specialized electronic equipment used to perform measurements with the I-VED technique consisted of the following devices:

- Variable frequency signal generator (20 MHz, 33220A, Agilent, Santa Clara, CA, USA)
- Data acquisition card (NI USB-6363, X Series Multifunction DAQ, National Instruments, Austin, TX, USA, 96 kHz/16 bit).
- Digital multimeter 51/2-digit (34405A, Agilent)
- Laptop (ASUSPRO, 4 GB RAM) with Sigview 5ch I-VED FFT v4.1 software.

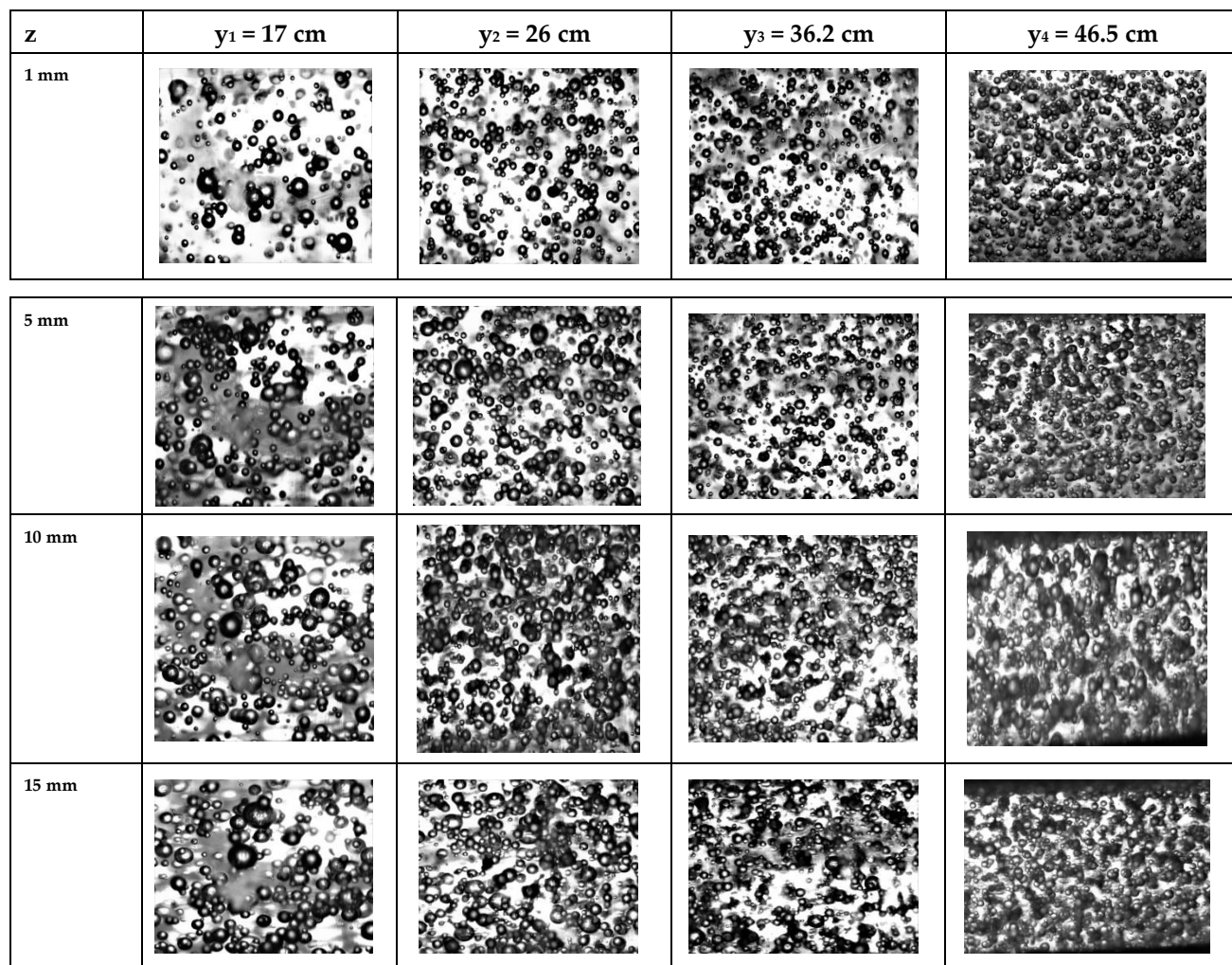
#### 2.2.4. Flow Field Investigation

An NaCl solution was utilized as a conductivity tracer for the estimation of the residence time distributions in an effort to study the mixing conditions inside the flotation column when a liquid jet was discharged. In particular, in this method, a high conductivity solution was injected into a solution with a lower conductivity and at the same time the electrical resistance of the mixture was measured locally at four different heights of the column, while dispersed air (0.7 L/min) was also inserted. Essentially, the time evolution of the electrical resistance developed described the flow field along the height of the column. Certainly, the presence of air bubbles strongly affected the flow field. The electrical resistance was measured using the electrical impedance technique I-VED using multiplexing, the principle of operation and measurement processing. With the use of multiplexing, the time evolution of the dispersion of the injection current in the liquid of the device in the four measurement channels of the gas phase fraction was simultaneously studied. In each experiment, the column contained an NaCl aqueous solution with a low specific conductivity (150–300  $\mu\text{S}/\text{cm}$ ) and 3 mL of an NaCl aqueous solution of higher specific conductivity (90 mS/cm) was injected into it. The solution was injected close to the bottom and centrally so that the dispersion was as homogeneous as possible. The sampling frequency of the measurements in the four channels was 25 kHz [60].

### 3. Results and Discussion

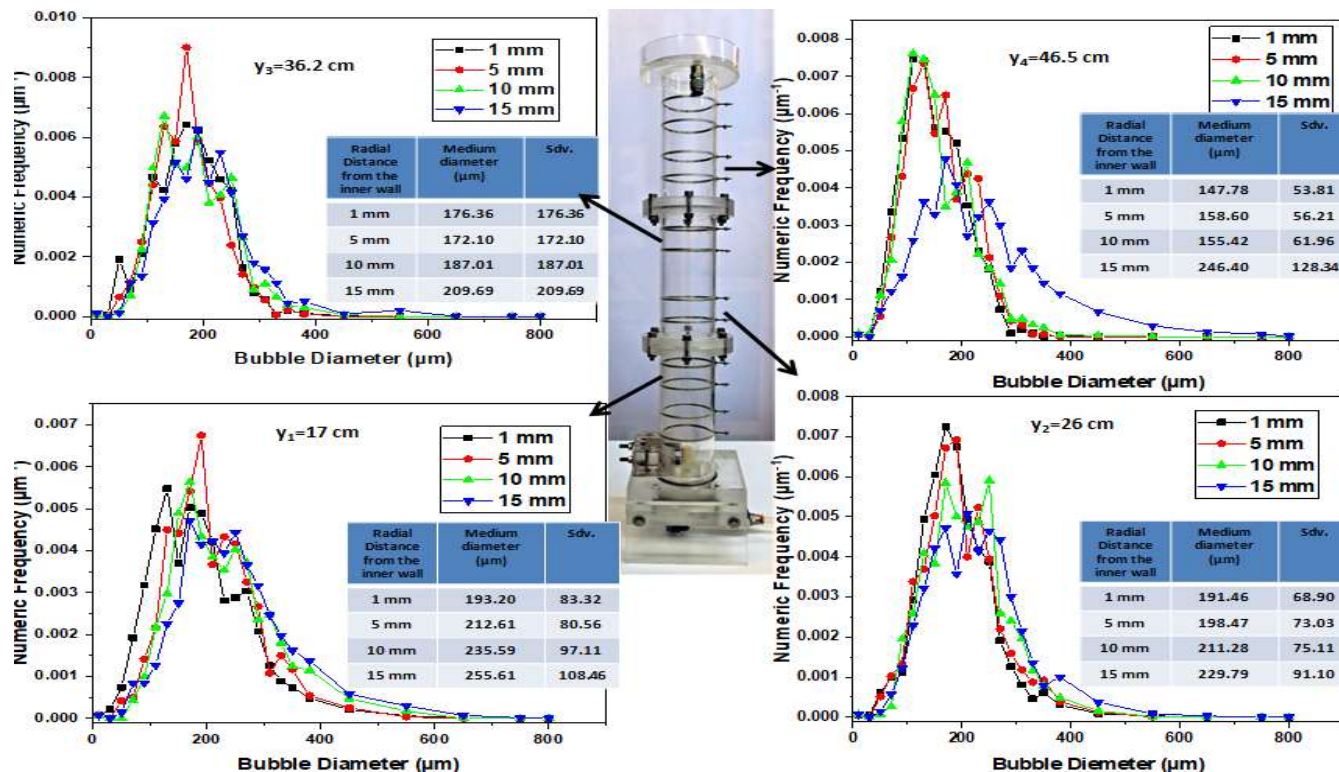
#### 3.1. Bubble Size Distribution

Figure 6 shows illustrative photographs of dispersed air bubbles in the flotation column in the presence of sodium oleate as the frother. The experiments were conducted at a concentration of 120 mg/L, which was the optimal amount during the flotation experiments realized using the same apparatus, when sodium oleate was used as the collector for magnesite particles [49]. The photographs were captured at a steady state for the four different heights of the column ( $y = 17, 26, 36.2$ , and  $46.5$  cm) and at four radial distances ( $z = 1, 5, 10$ , and  $15$  mm) from the inner wall of the column.



**Figure 6.** Dispersed air bubble images at four different heights  $y = 17, 26, 36.2$ , and  $46.5$  cm; four radial distances 1, 5, 10, and 15 mm from the column inner wall; and  $[SO] = 120$  mg/L.

Capturing pictures at different radial distances aimed to study the dispersion of the bubbles in the cross-section of the two-phase flow inside the flotation column. Visual observation of the indicative photos showed that the dispersion of the bubbles was not radially homogeneous, as the density of the bubble population appeared to be lower near the walls compared with the number of bubbles at the center of the column. Figure 7 presents the corresponding bubble size distributions for all positions and radial distances and, more specifically, shows the average diameter ( $dB_{av}$ ) and the standard deviation ( $StDev (dB_{av})$ ) for each distribution. It is worth mentioning that for each distribution, at least 500 bubbles were processed in order for the average calculated size to be statistically correct.

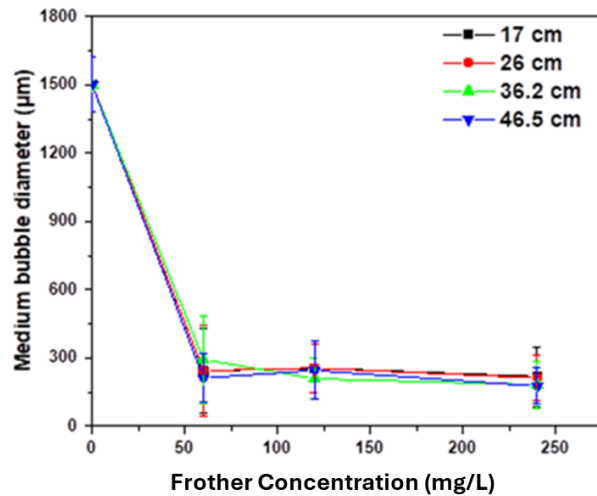


**Figure 7.** Bubble size distributions at four different heights  $y = 17, 26, 36.2$ , and  $46.5 \text{ cm}$ ; four radial distances 1, 5, 10, and 15 mm from the column inner wall; dispersed air, and  $[\text{SO}] = 120 \text{ mg/L}$ .

The results showed that at the lowest height of  $y_1 = 17 \text{ cm}$  and at a distance of 1 mm from the inner wall, the average size of the bubbles was  $148 \mu\text{m} (\pm 54)$ , while at a radial distance of 15 mm, it was  $246 \mu\text{m} (\pm 128)$ . Regarding the position  $y_2 = 26 \text{ cm}$  near the wall of the column, the average bubble size was  $191 \mu\text{m} (\pm 69)$ , while closer to the center (radial distance 15 mm) it was  $230 \mu\text{m} (\pm 91)$ . The trend of increasing in size while moving radially towards the center of the column followed from the data derived from the pictures captured in position  $y_3 = 36.2 \text{ cm}$ : close to the inner wall, the average size of the bubbles was  $176 \mu\text{m} (\pm 62)$ , while at a radial distance of 15 mm, it was  $210 \mu\text{m} (\pm 90)$ . In addition, the bubble distributions of the highest position ( $y_4 = 46.5 \text{ cm}$ ) appeared to follow the same trend. Near the wall, the average size was  $148 \mu\text{m} (\pm 54)$ , while closer to the center it was  $246 \mu\text{m} (\pm 128)$ . Generally, it was observed that in all four vertical positions of the column, the largest bubbles were located close to the center of the column, while the smaller bubbles were closer to the walls. This was attributed to the fact that the coarser bubbles rose rapidly in the center of the column, driving the smaller ones through recirculation to settle near the walls. The bubbles in the center line drew the liquid upwards. This created an imbalance and thus caused a kind of recirculation, and the liquid closer to the center flowed upwards while that closer to the wall flowed downwards. If the velocity of the downflow was greater than the relative velocity  $u_b$  of the bubbles, the bubbles appeared to move downwards [61]. Finally, no aggregation of the bubbles was observed along the height of the column, as the size of the bubbles did not seem to increase significantly at the highest locations. When the bubbles “met”, they bounced off each other without agglomerating because of the presence of the adsorbed frother on their surface [62].

Figure 8 outlines the effect of the frother concentration on the average diameter of the dispersed air bubbles for the four heights, and in particular for the radial position  $z_4 = 15 \text{ mm}$ , which was judged to be the most representative position of the two-phase flow. The experimental data depict that the average size of the bubbles decreased when the frother concentration increased and did not change significantly in height [63]. It was

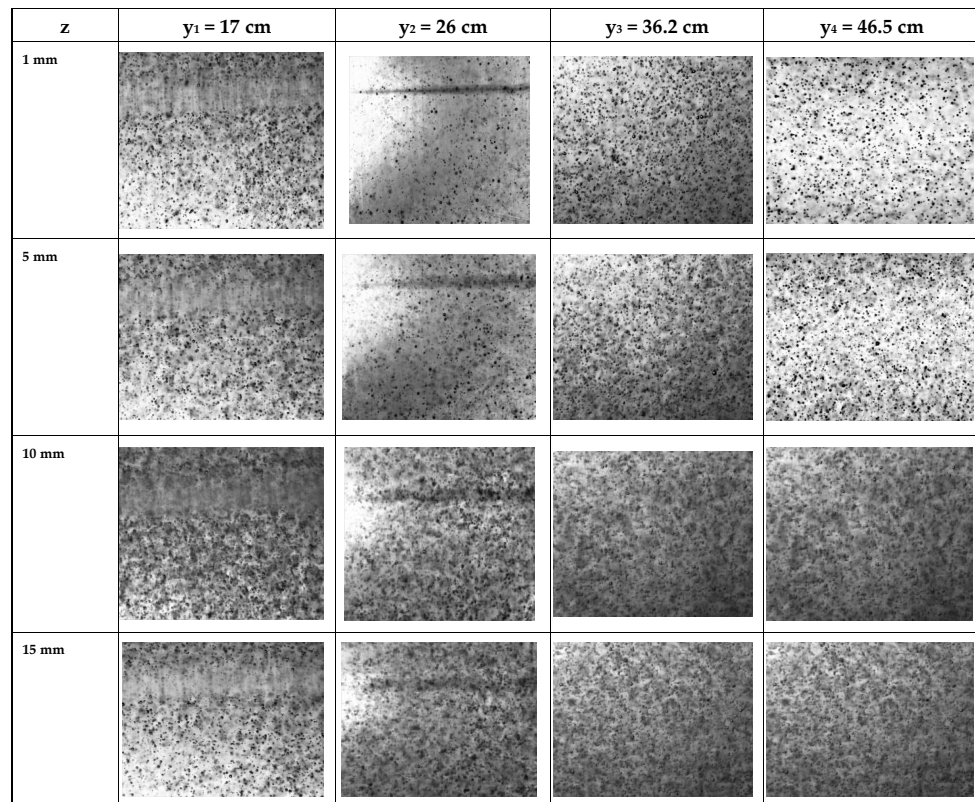
generally observed that the same trend was followed for the bubble size, both vertically and radially, for the different positions in the column.



**Figure 8.** Effect of frother concentration on the average bubble diameter; dispersed air; and  $[SO] = 0, 60, 120$ , and  $240 \text{ mg/L}$ .

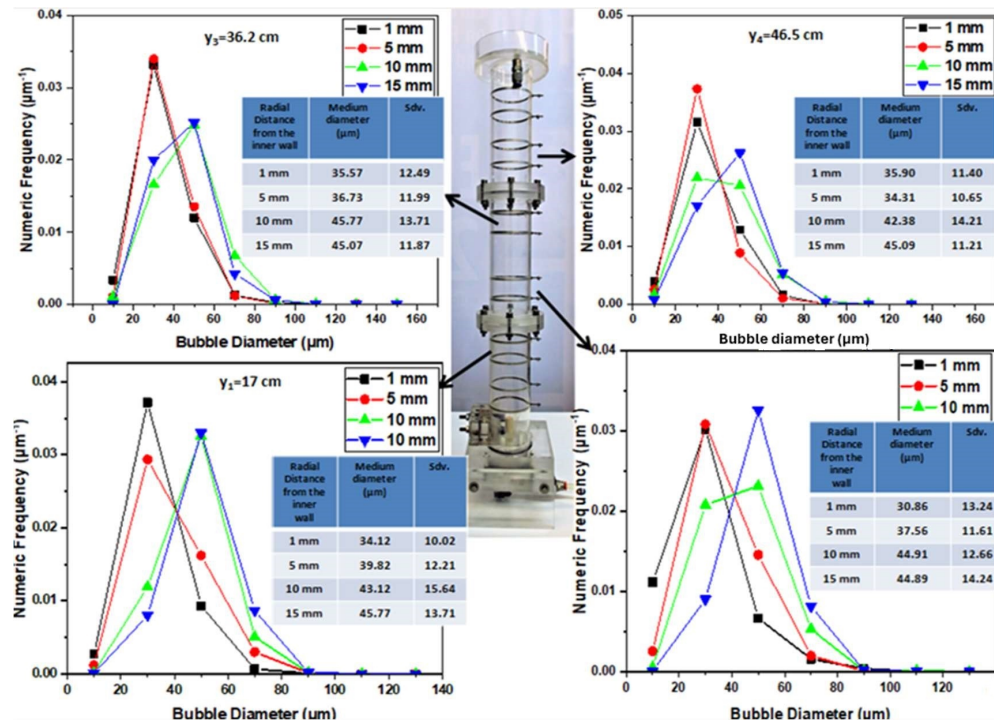
The presence of the surfactant led the solution surface tension decrease, resulting in a noticeable reduction in the bubbles size compared with the bubbles in the absence of a frother.

Indicative photographs of the bubbles produced with electrolysis of water in the flotation column in the presence of NaCl electrolyte ( $0.1 \text{ M}$ ) are presented in Figure 9. The photos were captured at the four aforementioned heights and radial distances of the column at steady state to study the dispersion of the electrolytic bubbles in the two-phase flow.



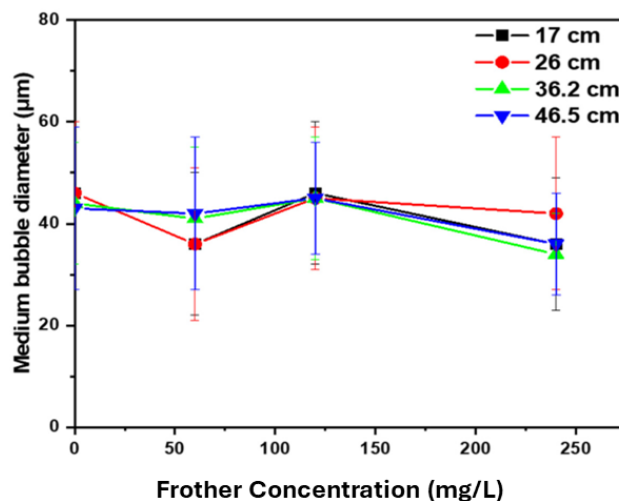
**Figure 9.** Electrolytic air bubble images at four different heights  $y = 17, 26, 36.2$ , and  $46.5 \text{ cm}$ ; four radial distances  $1, 5, 10$ , and  $15 \text{ mm}$  from the column inner wall;  $[SO] = 120 \text{ mg/L}$ ; and  $[\text{NaCl}] = 0.1 \text{ M}$ .

Figure 10 shows the bubble size distributions. The observation of the photos led to the assumption that the distribution of electrolytic bubbles was homogeneous, both vertically and radially.



**Figure 10.** Bubble size distributions at four different heights  $y = 17, 26, 36.2$ , and  $46.5 \text{ cm}$ ; four radial distances 1, 5, 10, and 15 mm from the column inner wall; electrolytic air;  $[\text{SO}] = 120 \text{ mg/L}$ ; and  $[\text{NaCl}] = 0.1 \text{ M}$ .

In summary, Figure 11 indicates the results of the effect of the concentration of the sodium oleate frother on the average size of the electrolytic air bubbles in the flotation column for the four positions along the height of the column for the radial position  $z_4 = 15 \text{ mm}$ , which was considered the most representative of the flow. The average bubble size decreased slightly with increasing the frother concentration and did not change appreciably at the different vertical positions.



**Figure 11.** Effect of frother concentration on the average bubbles diameter; electrolytic air;  $[\text{SO}] = 0, 60, 120$ , and  $240 \text{ mg/L}$ ; and  $[\text{NaCl}] = 0.1 \text{ M}$ .

### 3.2. Volumetric Gas Fraction

Under the framework of studying the hydrodynamic characteristics of the hybrid electroflotation column, the effect of the frother concentration on the volumetric gas fraction of the dispersed air was examined. Figure 12 presents the time series of the gas fraction for the four different heights of the flotation column ( $y = 17, 26, 36.2$ , and  $46.5$  cm) in the presence of sodium oleate (120 mg/L). In the first minute, the recorded fraction was zero and did not change, as no air was introduced to the column. In the sixth second, a sharp increase in the volume fraction was observed, while the two-phase system reached a steady state 50 s after the introduction of air. Air entrainment took place for 5 min, and the mean value of the volumetric gas fraction from the measurements recorded in the steady state region of each time series for locations  $y_1 = 17$  cm,  $y_2 = 26$  cm,  $y_3 = 36.2$  cm, and  $y_4 = 46.5$  cm was 5.4%, 5.6%, 5.8%, and 8%, respectively. The signals obtained in the presence of the highest frother concentration differed regarding the frequency of the peaks, compared with the signals with a lower oleate concentration.

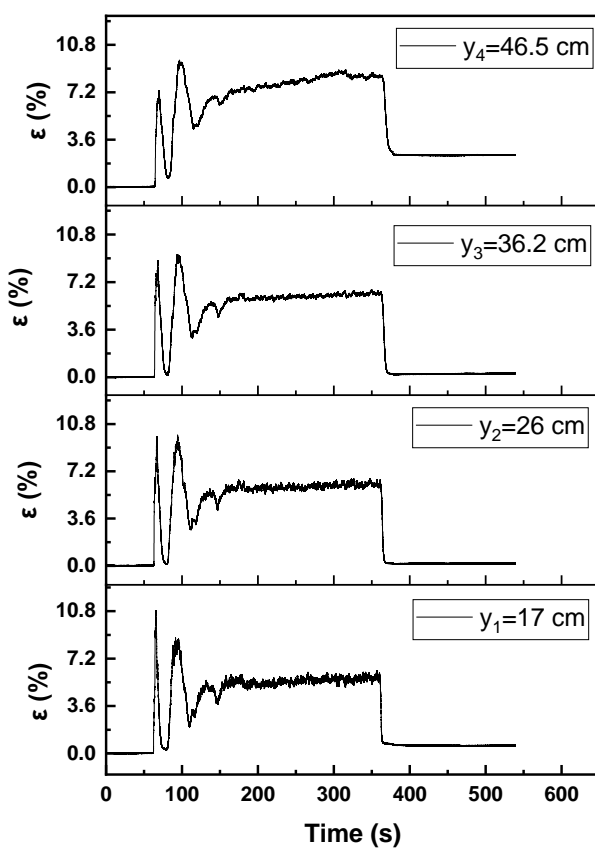


**Figure 12.** Gas fraction ( $\epsilon$ ) time evolution at four different heights  $y = 17, 26, 36.2$ , and  $46.5$  cm; dispersed air;  $[SO] = 120$  mg/L; and  $0.7$  L/min.

The time that each height reached steady state varied by 1 s and the positions near the porous sparger achieved a steady state quicker. Because of buoyancy, the bubbles moved with a relative velocity to the liquid and thus had their own dynamics. Because of this, the gas phase fraction reached a steady state faster than the liquid flow.

Figure 13 shows the effect of the frother concentration (0, 60, 120, and 240 mg/L) on the variations in the electrical signal of the volumetric gas fraction during 10 s of injection (steady state). The peak signals in the presence of 60 mg/L sodium oleate depicted a higher intensity and this was attributed to the larger sized individual bubbles, which increased at a higher speed. Furthermore, when the frother concentration was 120 mg/L, the volumetric fraction was higher as the smaller bubbles that formed had a longer residence time in

the column. Combining the data derived from the bubble size distributions at the same concentrations with the electrical signal measurements to calculate the volume fraction of the gas phase, it was concluded that the presence of smaller bubbles led to larger fractions as smaller bubbles had a longer residence time in the column due to a lower buoyancy speed, as already mentioned.

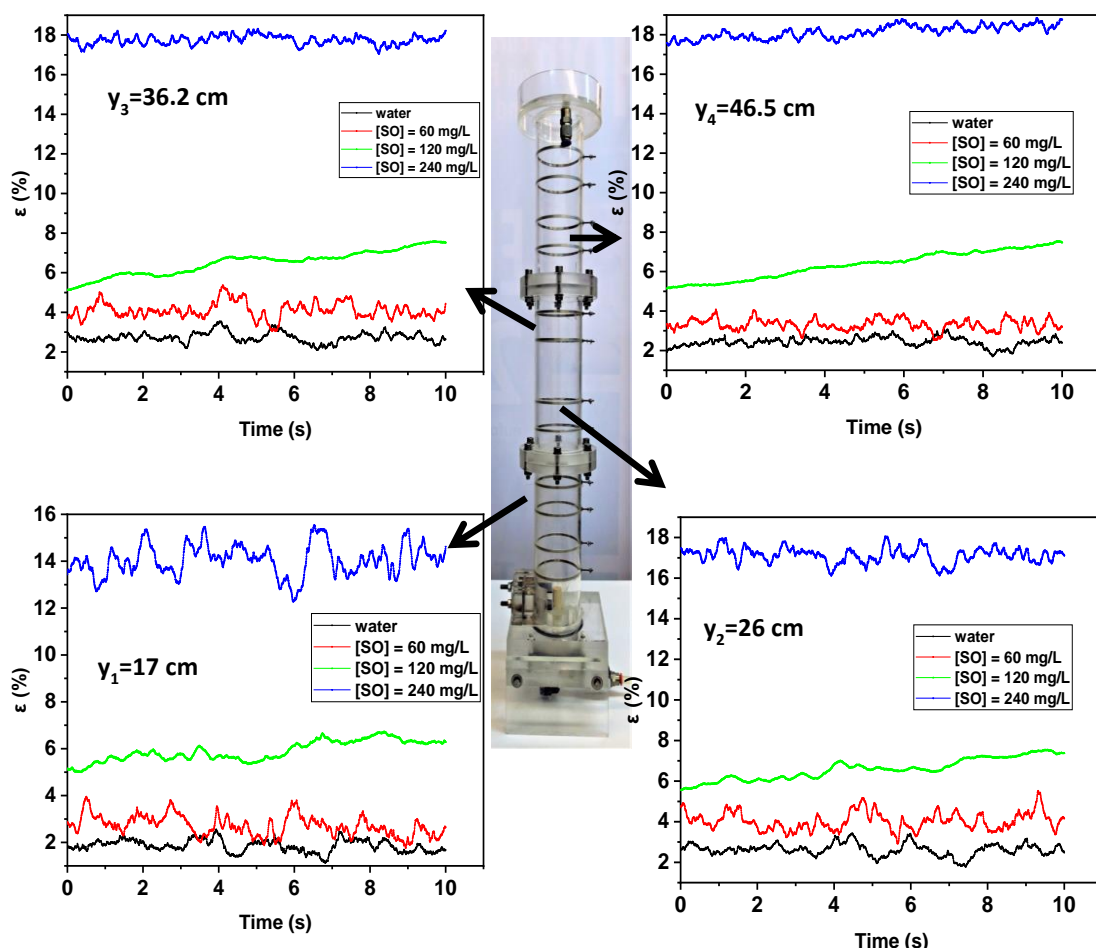


**Figure 13.** Gas fraction ( $\epsilon$ ) fluctuations with time under different frother concentrations, at four different heights  $y = 17, 26, 36.2$ , and  $46.5$  cm; dispersed air;  $[SO] = 0, 60, 120$ , and  $240$  mg/L; and  $0.7$  L/min.

Moreover, the difference observed in the values of the gas fractions could also be attributed to the limited movement of the bubbles due to the adsorbed layer of the frother. More specifically, the coefficient of the drag force exerted on the bubbles increased, and as a result, the buoyancy speed decreased, which led to recording higher volumetric fractions [64]. The fact that the electrical signals were in line with the optical measurements proves that although a photograph represented the instantaneous state of the two-phase flow, the information it contained was sufficient to describe the phenomenon overall.

Figure 14 presents the effect of the frother concentration on the evolution of the gas fraction in the height of the flotation column. The final volume fraction of the gas phase ( $\epsilon_f$ ) was calculated from the average values of the last measurements of the steady state region from each time series in Figure 12. Apart from indicating the values of the gas fraction, the electrical signals could furthermore be utilized to qualitatively characterize the two-phase flow. Initially, Kostoglou et al. theoretically studied the interactions between adjacent bubbles in two-phase flow as a first attempt to characterize their size through electrical signal fluctuations [65]. Then, Evgenidis and Karapantsios demonstrated experimentally that the intensity and frequency of fluctuations around the mean value of the air volume fraction,

in a two-phase flow with constant liquid and gas phase supply, depended on the mean bubble size [66]. More specifically, they developed an empirical relationship according to which the ratio of the standard deviation to the mean value of the air volumetric fraction ( $\text{StDev}(\varepsilon_{\text{av}})/\varepsilon_{\text{av}}$ ) increased with increasing the bubble size of the two-phase medium. The above possibility will be explored in the future.

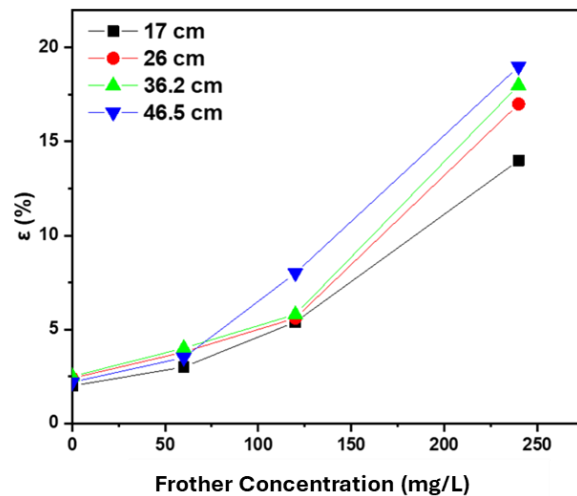


**Figure 14.** Mean gas fraction ( $\varepsilon$ ) at various frother concentrations; dispersed air;  $[\text{SO}] = 0, 60, 120$ , and  $240 \text{ mg/L}$ ; and  $0.7 \text{ L/min}$ .

### 3.3. Intensity of Bubble-Induced Scattered Light Method

To characterize the gas phase of the flotation system in the hybrid flotation column, experiments were carried out using the scattered light optical method. Figure 15 shows the time series of the light energy intensity ( $W(t)$ ) for the four vertical positions of the flotation column in the presence of dispersed air in the absence of a frother and in the presence of three different concentrations, 60, 120 and 240 mg/L.

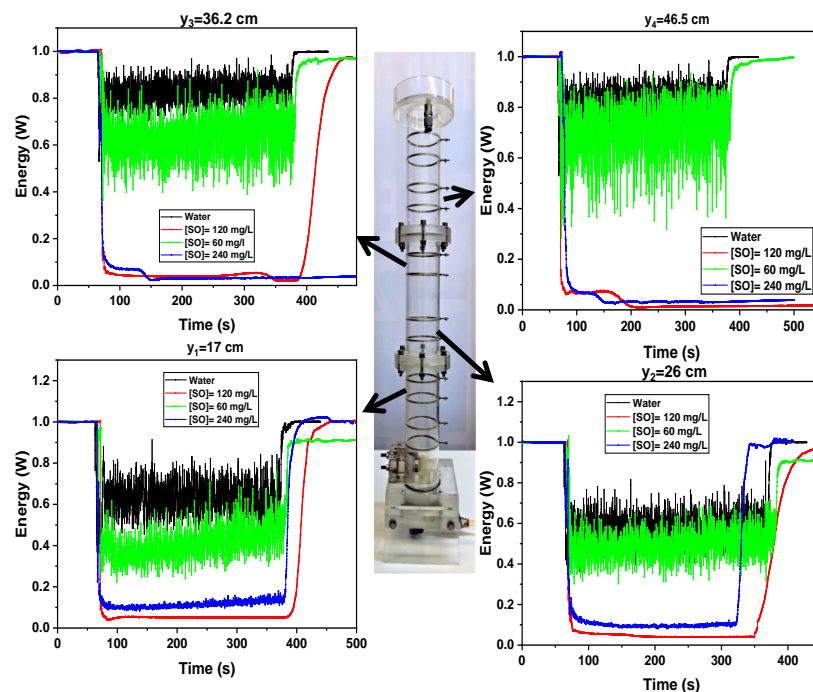
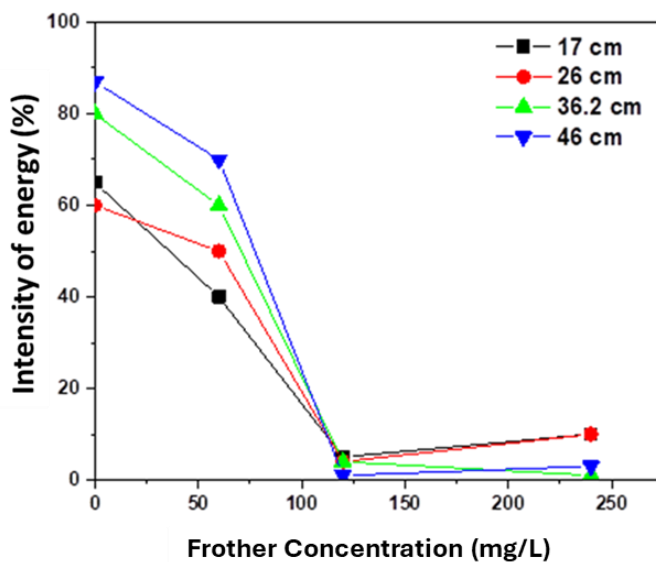


**Figure 15.** Change in energy intensity at four different heights  $y = 17, 26, 36.2$ , and  $46.5 \text{ cm}$ ; dispersed air;  $[\text{SO}] = 0, 60, 120$ , and  $240 \text{ mg/L}$ ;  $0.7 \text{ L/min}$ .

In the first 60 s of the measurement, the intensity of light that passed from one side of the device to the other before the introduction of air (baseline) was recorded. The light intensity of the single-phase medium was constant with time as the composition of the slurry did not change, and thus no diffusion of the energy occurred. The air intake (0.7 L/min) after 60 s was accompanied by a sharp drop in light intensity. The light diffused over the dispersed air bubbles it encountered along its path and the energy of the light beam exiting the other wall of the device became less than that of the light source. Air was introduced for 5 min and a steady state was achieved after about 10 s. Moreover, it was observed that at the end of the air intake and, in particular, regarding the higher position,  $y_4$  did not return to its initial state (single-phase medium) as foam had formed, resulting in the impossible gradual restoration of the energy to the levels of the single-phase liquid medium.

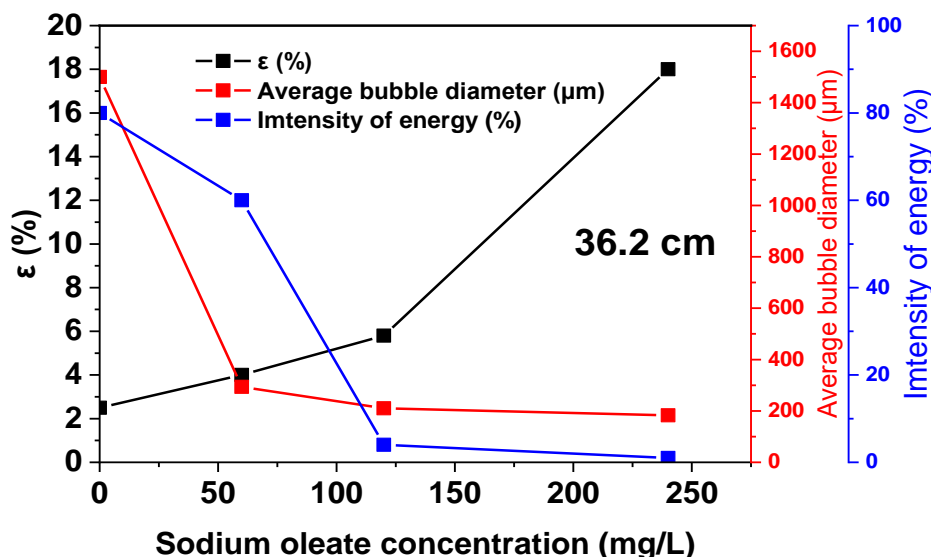
We conducted a comparative study to manage the effect of the frother concentration on the change in the energy of the light source for the four vertical positions in the presence of dispersed air. As mentioned, the concentrations we studied were 60, 120, and 240 mg/L. The results depict that a smaller change in energy took place in the presence of water (20–40%) with the lowest frother concentration (40–60%), while as the concentration of oleate increased, the change reached 90%. It was obvious that the change in energy depended on the size of the bubbles of the gas phase and, more specifically, the larger the size of the bubbles, the smaller the change in outward energy, as the light diffused less. In addition, the smaller bubbles moved in the bulk and covered the entire volume of the column, causing the light to diffuse intensely; therefore, a greater change in the recorded energy was observed [67]. The decrease in the light intensity appeared to be uniform for all four vertical positions of the column. This shows that the gas phase was homogeneously distributed along the height of the column and, furthermore, the average size of the bubbles and their distribution did not differ significantly in the different positions.

Figure 16 shows the transmitted energy (%) of the light source due to scattering in the flotation column for various column heights and frother concentrations in presence of dispersed air. The greatest energy reduction was observed at the highest position of the column ( $y_4 = 46.5$  cm). It was observed that at the highest positions and for sodium oleate concentrations of 120 and 240 mg/L, a small percentage of energy that reached the opposite side of the column was recorded, as the average bubble size was smaller due to a reduction in the surface tension.



**Figure 16.** Effect of the frother concentration on the change in energy intensity at four different heights  $y = 17, 26, 36.2$ , and  $46.5$  cm; dispersed air;  $[SO] = 0, 60, 120$ , and  $240$  mg/L;  $0.7$  L/min.

Figure 17 summarizes the results of the hydrodynamic study on the flotation column regarding the effect of the frother concentration (red line) on the average size of the dispersed air bubbles, (black line) on the time series of the volumetric gas fraction, and (blue line) the energy of the light source that passes through the bulk due to diffusion, for the four different positions of the column in height. It can be concluded that at the highest positions,  $y_3$  and  $y_4$ , the increase in the concentration of the frother led to an increase in the volumetric gas fraction, while the recorded energy of the light that reached the detector was lower due its diffusion at the bubble surfaces. The average bubble size decreased with increasing the concentration; however, it did not change significantly at the different vertical positions of the column. The measurements were conducted simultaneously.



**Figure 17.** Pivot graph of the frother concentration effect on the (red line) bubble size distributions, (black line) mean gas fraction, (blue line) change in light intensity due to diffusion at  $y = 36.2$  cm, and dispersed air.

### 3.4. Flow Dispersion

Figure 18 presents the evolution of the electrical resistance of the dispersion as countered by the electrode pairs. The evolution of the electrical resistance was due to the conducting tracer injected in the flow field and it was representative of the residence time distributions of the injection stream in the flotation column at the four different height positions in the presence of sodium oleate (120 mg/L) and dispersed air flow (0.7 L/min). Once a steady state was accomplished, the tracer was injected close to the ceramic sparger in order to ensure a representative “picture” of the two-phase flow inside the column. Figure 18a shows that the dispersion of the tracer in the working solution was distributed uniformly in the volume of the column, while Figure 18b shows that the injection current was dispersed along the height of the column and reached the four positions with a time difference equal to 1 s, while a steady state (plateau) occurred after 7 s. The presence of bubbles in the flow affected the residence time distribution of the liquid in the column in two ways; initially, by forcing the dispersion of the tracer and, additionally, by controlling the time required to restore equilibrium at different heights. As the bubbles rose to the free surface of the liquid, a velocity profile was created around them, and thus the dispersion of the injection stream in the column liquid was enhanced.

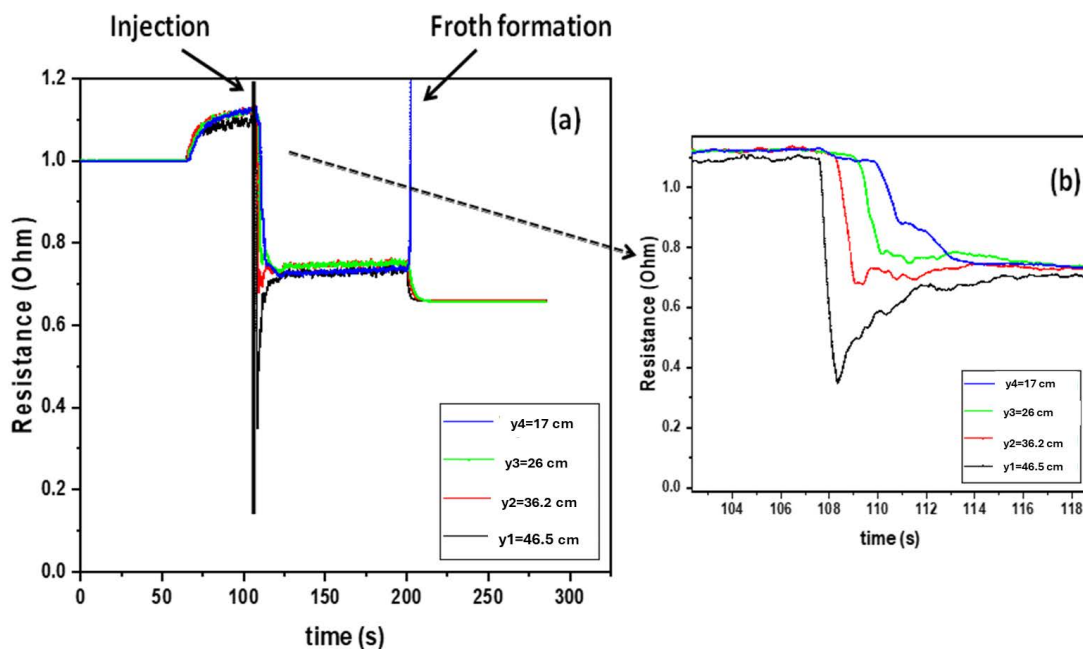


**Figure 18.** (a) Evolution of the conducting tracer induced electrical resistance for the four different heights  $y = 17, 26, 36.2$ , and  $46.5$  cm; dispersed air;  $[SO] = 120$ ; and  $0.7$  L/min. (b) Magnification of the curves around the injection moment.

#### 4. Conclusions

In the present work, an experimental study of some of the hydrodynamic characteristics of a hybrid electroflotation column was conducted. For this purpose, optical and electrical methods were utilized to investigate the bubble size distributions, the volumetric gas fraction, and the flow field evolution in the hybrid column.

The experimental results can be concluded as follows:

- The study of the size distribution of the bubbles in the flotation column showed that at the four vertical positions of the column, coarser bubbles appeared in the center of the column, while smaller bubbles appeared closer to the walls through the recirculation zone near the walls. The average bubble size decreased when the frother concentration increased and did not change considerably at the different vertical positions. In general, that trend was observed both vertically and radially for the different positions in the column. Moreover, no coalescence of the bubbles was observed.
- The measurement of the volume fraction showed that the presence of smaller bubbles led to larger air fractions due to a lower buoyancy velocity and an increase in frother concentration as the volume fraction increased.
- The experiments realized with the scattered light optical method for correlating the bubble size and number showed that an increase in frother concentration caused a greater change in the energy of the light source passing through the flotation devices, due to diffusion over smaller and numerous bubbles.
- The study of the residence time distribution in the flotation column depicted that the dispersion led to a uniform trace concentration along the column and the steady state occurred 3 s after the dispersed air was inserted.

**Author Contributions:** Conceptualization, M.K., T.D.K. and N.K.L.; data curation, P.K.T.; investigation, P.K.T.; supervision, M.K., T.D.K. and N.K.L.; writing—original draft, P.K.T.; writing—review and editing, M.K., T.D.K. and N.K.L. All authors have read and agreed to the published version of the manuscript.

**Funding:** The present research was funded by the European Union’s Horizon 2020 research and innovation program under grant agreement No. 821265—FineFuture.

**Data Availability Statement:** The data presented in this study are available upon request from the corresponding authors.

**Acknowledgments:** The authors would like to acknowledge Grecian Magnesite for providing magnesite samples for this study.

**Conflicts of Interest:** The authors declare that they have no known competing financial interests or personal relationships that could have appeared to influence the work reported in this paper.

## References

1. Sriram, K.; Mann, R. Dynamic gas disengagement: A new technique for assessing the behaviour of bubble columns. *Chem. Eng. Sci.* **1977**, *32*, 571–580. [\[CrossRef\]](#)
2. Jena, M.S.; Biswal, S.K.; Das, S.P.; Reddy, P.S.R. Comparative study of the performance of conventional and column flotation when treating coking coal fines. *Fuel Process. Technol.* **2008**, *89*, 1409–1415. [\[CrossRef\]](#)
3. Islam, M.T.; Nguyen, A.V. Effect of microturbulence on bubble-particle collision during the bubble rise in a flotation cell. *Miner. Eng.* **2020**, *155*, 106418. [\[CrossRef\]](#)
4. Darabi, H.; Koleini, S.M.J.; Deglon, D.; Rezai, B.; Abdollahy, M. Particle Image Velocimetry Study of the Turbulence Characteristics in an Aerated Flotation Cell. *Ind. Eng. Chem. Res.* **2017**, *56*, 13919–13928. [\[CrossRef\]](#)
5. Nesse, T.; Heinrich, S.H.; Mockel, O. Tubulenzmessung in Mehrphasenstromungen gasformig/flüssig und fest/flüssig mittels einer Piezsonde. In Proceedings of the 2nd European Symposium on Particle Measurement Techniques, Nürnberg, Germany, 24–26 September 1979.
6. Newell, R.; Grano, S. Hydrodynamics and scale up in Rushton turbine flotation cells: Part 2. flotation scale-up for laboratory and pilot cells. *Int. J. Miner. Process.* **2006**, *81*, 65–78. [\[CrossRef\]](#)
7. Schubert, H. On the optimization of hydrodynamics in fine particle flotation. *Miner. Eng.* **2008**, *2*, 930–936. [\[CrossRef\]](#)
8. Deglon, D.A.; Egya-mensah, D.J.; Franzidis, P. Review of Hydrodynamics and Gas Dispersion in Flotation Cells on South African Platinum Concentrators. *Miner. Eng.* **2000**, *13*, 235–244. [\[CrossRef\]](#)
9. Schwarz, S.; Alexander, D. Gas dispersion measurements in industrial flotation cells. *Miner. Eng.* **2006**, *19*, 554–560. [\[CrossRef\]](#)
10. Laplante, A.R.; Toguri, J.M.; Smith, H.W. The Effect of Air Flow Rate on the Kinetics of Flotation. Part 2: The Transfer of Material from the Froth over the Cell Lip. *Int. J. Miner. Process.* **1983**, *11*, 221–234. [\[CrossRef\]](#)
11. Ata, S. Phenomena in the Froth Phase of Flotation—A Review. *Int. J. Miner. Process.* **2011**, *102*, 1–12. [\[CrossRef\]](#)
12. Hadler, K.; Greyling, M.; Plint, N.; Cilliers, J.J. The Effect of Froth Depth on Air Recovery and Flotation Performance. *Miner. Eng.* **2012**, *36–38*, 248–253. [\[CrossRef\]](#)
13. Ahmed, N.; Jameson, G.J. Flotation kinetics. *Miner. Process. Extr. Metall.* **1989**, *5*, 77–99. [\[CrossRef\]](#)
14. Power, A.; Franzidis, J.P.; Manlapig, E.V. The characterisation of hydrodynamic conditions in industrial flotation cells. In Proceedings of the AusIMM’4 7th Mill Operators Conference, Australasian Institute of Mining and Metallurgy, Kalgoorlie, Australia, 12–14 October 2000; pp. 243–255.
15. Deng, H.; Mehta, R.K.; Warren, G.W. Numerical modeling of flows in flotation columns. *Int. J. Miner. Process.* **1996**, *48*, 61–72. [\[CrossRef\]](#)
16. Xia, Y.K.; Peng, F.F.; Wolfe, E. CFD simulation of alleviation of fluid back mixing by baffles in bubble column. *Miner. Eng.* **2006**, *19*, 925–937. [\[CrossRef\]](#)
17. Koh, P.T.L.; Schwarz, M.P. CFD model of a self-aerating flotation cell. *Int. J. Miner. Process.* **2007**, *85*, 16–24. [\[CrossRef\]](#)
18. Zargaran, A.; Mozaffari, E.; Giddings, D. Gas-liquid slip velocity determination in co-current column flotation. *Sep. Purif. Technol.* **2016**, *169*, 179–186. [\[CrossRef\]](#)
19. Su, W.; Yan, X.; Wang, L.; Zhang, H.; Cao, Y. Effect of height of flotation column on flow field. *Asia Pac. J. Chem. Eng.* **2019**, *14*, 2311. [\[CrossRef\]](#)
20. Hoang, D.H.; Hassanzadeh, A.; Peuker, U.A.; Rudolph, M. Impact of flotation hydrodynamics on the optimization of fine-grained carbonaceous sedimentary apatite ore beneficiation. *Powder Technol.* **2019**, *345*, 223–233. [\[CrossRef\]](#)
21. Rodrigues, R.T.; Rubio, J. New basis for measuring the size distribution of bubbles. *Miner. Eng.* **2003**, *16*, 757–765. [\[CrossRef\]](#)
22. Zhou, Z.A.; Egiebor, N.O.; Plitt, L.R. Frother effects on bubble size estimation in a flotation column. *Miner. Eng.* **1993**, *6*, 55–67. [\[CrossRef\]](#)
23. Kim, S.; Kwon, O.; Seo, J.K.; Yoon, J.R. On a nonlinear partial differential equation arising in magnetic resonance electrical impedance tomography. *SIAM J. Math. Anal.* **2002**, *34*, 511–526. [\[CrossRef\]](#)
24. Cho, J.; Perlin, M.; Ceccio, S.L. Measurement of near-wall stratified bubbly flows using electrical impedance. *Meas. Sci. Technol.* **2005**, *16*, 1021. [\[CrossRef\]](#)
25. Sung, J.S.; Burgess, J.M. A laser-based method for bubble parameter measurement in two-dimensional fluidised beds. *Powder Technol.* **1987**, *49*, 165–175. [\[CrossRef\]](#)

26. Etchepare, R.; Azevedo, A.; Calgaroto, S.; Rubio, J. Removal of ferric hydroxide by flotation with micro and nanobubbles. *Sep. Purif. Technol.* **2017**, *184*, 347–353. [[CrossRef](#)]
27. Oh, S.H.; Kim, J.M. Generation and stability of bulk nanobubbles. *Langmuir* **2017**, *33*, 3818–3823. [[CrossRef](#)]
28. Zhang, X.Y.; Wang, Q.S.; Wu, Z.X.; Tao, D.P. An experimental study on size distribution and zeta potential of bulk cavitation nanobubbles. *Int. J. Miner. Metall. Mater.* **2020**, *27*, 152–161. [[CrossRef](#)]
29. Rowe, P.N.; Matsuno, R. Single bubbles injected into a gas fluidised bed and observed by X-rays. *Chem. Eng. Sci.* **1971**, *26*, 923–935. [[CrossRef](#)]
30. Kim, S.; Kim, H.; Han, M.; Kim, T. Generation of sub-micron (nano) bubbles and characterization of their fundamental properties. *Environ. Eng. Res.* **2019**, *24*, 382–388. [[CrossRef](#)]
31. Huang, S.; Wu, X.; Zong, B.; Ma, Y.; Guo, X.; Wang, D. Local Void Fractions and Bubble Velocity in Vertical Air-Water Two-Phase Flows Measured by Needle-Contact Capacitance Probe. *Sci. Technol. Nucl. Install.* **2018**, *2018*, 7532618. [[CrossRef](#)]
32. O’Neill, K.T.; Brancato, L.; Stanwix, P.L.; Fridjonsson, E.O.; Johns, M.L. Two-Phase Oil/Water Flow Measurement Using An Earth’s Field Nuclear Magnetic Resonance Flow Meter. *Chem. Eng. Sci.* **2019**, *202*, 222–237. [[CrossRef](#)]
33. Sankey, M.H.; Holland, D.J.; Sederman, A.J.; Gladden, L.F. Magnetic Resonance Velocity Imaging of Liquid and Gas Two-Phase Flow in Packed Beds. *J. Magn. Reson.* **2009**, *196*, 142–148. [[CrossRef](#)] [[PubMed](#)]
34. Chakraborty, S.; Keller, E.; Talley, J.; Srivastav, A.; Ray, A.; Kim, S. Void Fraction Measurement in Two-Phase Flow Processes Via Symbolic Dynamic Filtering of Ultrasonic Signals. *Meas. Sci. Technol.* **2009**, *20*, 023001. [[CrossRef](#)]
35. Al-lababidi, S.; Addali, A.; Yeung, H.; Mba, D.; Khan, F. Gas Void Fraction Measurement in Two-Phase Gas/Liquid Slug Flow Using Acoustic Emission Technology. *J. Vib. Acoust.* **2009**, *131*, 064501. [[CrossRef](#)]
36. Nazemi, E.; Feghhi, S.A.H.; Roshani, G.H.; Setayeshi, S.; Peyvandi, R.G. A Radiation-Based Hydrocarbon Two-Phase Flow Meter for Estimating of Phase Fraction Independent of Liquid Phase Density in Stratified Regime. *Flow Meas. Instrum.* **2015**, *46*, 25–32. [[CrossRef](#)]
37. Roshani, G.H.; Nazemi, E. A High Performance Gas-Liquid Two-Phase Flow Meter Based on Gamma-Ray Attenuation and Scattering. *Nuc Sci. Tech.* **2017**, *28*, 169. [[CrossRef](#)]
38. Olerni, C.; Jia, J.; Wang, M. Measurement of Air Distribution and Void Fraction of An Upwards Air-Water Flow Using Electrical Resistance Tomography and A Wire-Mesh Sensor. *Meas. Sci. Technol.* **2013**, *24*, 035403. [[CrossRef](#)]
39. Ofuchi, C.Y.; Eidt, H.K.; Rodrigues, C.C.; Dos Santos, E.N.; Dos Santos, P.H.D.; Da Silva, M.J.; Neves, F., Jr.; Domingos, P.V.S.R.; Morales, R.E.M. Multiple Wire-Mesh Sensors Applied to the Characterization of Two-Phase Flow inside a Cyclonic Flow Distribution System. *Sensors* **2019**, *19*, 193. [[CrossRef](#)]
40. DiFilippo, E.L.; Brusseau, M.L. Application of Light Reflection Visualization for Measuring Organic-Liquid Saturation for Two-Phase Systems in Two-Dimensional Flow Cells. *Environ. Eng. Sci.* **2011**, *28*, 803–809. [[CrossRef](#)]
41. Boschan, A.; Poblete, M.; Lucrecia Roht, Y.; Ippolito, I.; Chertcoff, R. Light Transmission Measurement of Solute Dispersion in Non-Brownian Suspension Flow. *Eur. Phys. J. Appl. Phys.* **2014**, *65*, 11101. [[CrossRef](#)]
42. Gamio, J.C.; Castro, J.; Rivera, L.; Alamilla, J.; Garcia-Nocetti, F.; Aguilar, L. Visualisation of gas-oil two-phase flows in pressurized pipes using electrical capacitance tomography. *Flow Meas. Instrum.* **2005**, *16*, 129–134. [[CrossRef](#)]
43. Wang, M. Electrode models in electrical impedance tomography. *J. Zhejiang Univ.-SCIENCE A* **2005**, *6*, 1386–1393. [[CrossRef](#)]
44. Devanathan, N.; Moslemian, D.; Dudukovic, M.P. Flow mapping in bubble columns using CARPT. *Chem. Engng Sci.* **1990**, *45*, 2285–2291. [[CrossRef](#)]
45. Sheng, S. New development in the technology of flow measurement over the last decade. *Mech. Eng.* **2002**, *24*, 1–14.
46. Ge, M.; Manikkam, P.; Ghossein, J.; Subramanian, R.K.; Coutier-Delgosha, O.; Zhang, G. Dynamic mode decomposition to classify cavitating flow regimes induced by thermodynamic effects. *Energy* **2022**, *254*, 124426. [[CrossRef](#)]
47. Ge, M.; Zhang, G.; Petkovšek, M.; Long, K.; Coutier-Delgosha, O. Intensity and regimes changing of hydrodynamic cavitation considering temperature effects. *J. Clean. Prod.* **2022**, *338*, 130470. [[CrossRef](#)]
48. Deng, W.; Xu, L.; Li, Z.; Tang, W.; Wang, X.; Shang, L.; Liu, D.; Liu, X. Stability Analysis of Vaneless Space in High-Head Pump-Turbine under Turbine Mode: Computational Fluid Dynamics Simulation and Particle Imaging Velocimetry Measurement. *Machines* **2022**, *10*, 143. [[CrossRef](#)]
49. Tsavet, P.K.; Kostoglou, M.; Karapantsios, T.D.; Lazaridis, N.K. A Hybrid device for enhancing flotation of fine particles by combining micro-Bubbles with conventional bubbles. *Minerals* **2021**, *11*, 561. [[CrossRef](#)]
50. Rulyov, N.N. Combined microflotation of fine minerals: Theory and experiment. mineral processing and extractive metallurgy. *Trans. Inst. Min. Metall. C* **2016**, *125*, 81–85.
51. Rulyov, N.N.; Tussupbayev, N.K.; Kravtchenko, O.V. Combined microflotation of fine quartz. Mineral processing and extractive metallurgy. *Trans. Inst. Min. Metall. C* **2015**, *124*, 217–233.
52. Rulyov, N.N.; Filippov, L.O.; Kravchenko, O.V. Combined microflotation of glass beads. *Colloids Surf. A Physicochem. Eng. Asp.* **2020**, *598*, 124810. [[CrossRef](#)]
53. Cho, Y.S.; Laskowski, J.S. Bubble coalescence and its effect on dynamic foam stability. *Can. J. Chem. Eng.* **2002**, *80*, 299–305. [[CrossRef](#)]
54. Zabulis, X.; Papara, M.; Chatziargyriou, A.; Karapantsios, T.D. Detection of densely dispersed spherical bubbles in digital images based on a template matching technique: Application to wet foams. *Colloids Surf. A Physicochem. Eng. Asp.* **2007**, *309*, 96–106. [[CrossRef](#)]

55. Chan, B.S.; Tsang, Y.H. A theory on bubble-size dependence of the critical electrolyte concentration for inhibition of coalescence. *J. Colloid Interface Sci.* **2005**, *286*, 410–413. [[CrossRef](#)] [[PubMed](#)]
56. Gorain, B.K.; Franzidis, J.P.; Manlapig, E.V. Studies on impeller type, impeller speed and air flow rate in an industrial scale flotation cell. Part 4: Effect of bubble surface area flux on flotation performance. *Miner. Eng.* **1997**, *10*, 367–379. [[CrossRef](#)]
57. Karapantsios, T.D.; Evgenidis, S.P.; Zacharias, K.; Mesimeris, T. Method for the Detection and Characterization of Bubbles in Liquids and Device Therefore, Resp. System. *Eur. Patent Office* **2016**, 3005942, A1.
58. Tsochatzidis, N.A.; Karapantsios, T.D.; Kostoglou, M.V.; Karabelas, A.J. A conductance probe for measuring liquid fraction in pipes and packed beds. *Int. J. Multiph. Flow* **1992**, *18*, 653–667. [[CrossRef](#)]
59. Karapantsios, T.D.; Paras, S.V.; Karabelas, A.J. Statistical characteristics of free fallinf films at high Reynolds numbers. *Int. J. Multiph. Flow* **1989**, *15*, 1–21. [[CrossRef](#)]
60. Evgenidis, S.P.; Karapantsios, T.D. Effect of bubble size on void fraction fluctuations in dispersed bubble flows. *Int. J. Multiph. Flow* **2015**, *75*, 163–173. [[CrossRef](#)]
61. Benilov, E.S.; Cummins, C.P.; Lee, W.T. Why do bubbles in Guinness sink? *Am. J. Phys.* **2013**, *81*, 88–91. [[CrossRef](#)]
62. Doran, P.M. *Physical Processes in Bioprocess Engineering Principles*, 2nd ed.; Academic Press: San Diego, CA, USA, 2013.
63. Evgenidis, S.P.; Kazakis, N.A.; Karapantsios, T.D. Bubbly flow characteristics during decompression sickness: Effect of surfactant and electrolyte on bubble size distribution. *Colloids Surf. A Physicochem. Eng. Asp.* **2010**, *365*, 46–51. [[CrossRef](#)]
64. Fossa, M. Design and performance of a conductance probe for measuring the liquid fraction in two-phase gas-liquid flows. *Flow Meas. Instrum.* **1998**, *9*, 103–109. [[CrossRef](#)]
65. Kostoglou, M. On the effect of flowing circular entities swarms on strip electrodes conductance. *Ind. Eng. Chem. Res.* **2012**, *51*, 5615–5625. [[CrossRef](#)]
66. Evgenidis, S.P.; Kostoglou, M.; Karapantsios, T.D. Study of void fraction fluctuations dependence on bubble size through experimental and simulated electrical signal analysis. In Proceedings of the Smart and Green Interfaces 2016, Athens, Greece, 4–6 May 2016.
67. Nguyen, P.T.; Hampton, M.A.; Nguyen, A.V.; Birkett, G.R. The influence of gas velocity, salt type and concentration on transition concentration for bubble coalescence inhibition and gas holdup. *Chem. Eng. Res. Des.* **2012**, *90*, 33–39. [[CrossRef](#)]

**Disclaimer/Publisher’s Note:** The statements, opinions and data contained in all publications are solely those of the individual author(s) and contributor(s) and not of MDPI and/or the editor(s). MDPI and/or the editor(s) disclaim responsibility for any injury to people or property resulting from any ideas, methods, instructions or products referred to in the content.